Liquid Crystals
Publication details, including instructions for authors and subscription information:
http://www.informaworld.com/smpp/title~content=t713926090

The investigation of the relaxation processes in antiferroelectric liquid crystals by broad band dielectric and electro-optic spectroscopy

Yu. P. Panarin; O. Kalinovskaya; J. K. Vij

Online publication date: 06 August 2010

To cite this Article Panarin, Yu. P. , Kalinovskaya, O. and Vij, J. K.(1998) 'The investigation of the relaxation processes in antiferroelectric liquid crystals by broad band dielectric and electro-optic spectroscopy', Liquid Crystals, 25: 2, 241 — 252
To link to this Article: DOI: 10.1080/026782998206399
URL: http://dx.doi.org/10.1080/026782998206399

LIQUID CRYSTALS, 1998, VOL. 25, NO. 2, 241–252

The investigation of the relaxation processes in antiferroelectric liquid crystals by broad band dielectric and electro-optic spectroscopy

by YU. P. PANARIN, O. KALINOVSKAYA and J. K. VIJ*

Department of Electronic and Electrical Engineering, Trinity College, University of Dublin, Dublin 2, Ireland

(*Received 6 January 1998; in final form 2 March 1998; accepted 20 March 1998*)

Wide band dielectric and electro-optic spectroscopy of an antiferroelectric liquid crystal (AFLC) has been carried out over a range of frequencies from 1 kHz to 1 GHz. The AFLC sample under investigation possesses a variety of different ferri-, ferro-, and antiferro-electric phases. Dielectric spectroscopy of the LC cells in the antiferroelectric phases reveals both collective and individual dynamics of molecules. In the antiferroelectric SmC_A phase, three dielectric relaxation processes are found in the absence of the bias and an additional relaxation process appears under the bias field. A solution of the dynamical equation of the director subject to a weak alternating field for the anitferroelectric helix has been found. A comparison of the results of electro-optic and dielectric spectroscopy with a theoretical study enables a determination of the origin of the relaxation processes in antiferroelectric phases. The mechanism for the distortion of the antiferroelectric helix has been determined using dielectric spectroscopy and a non-linear electro-optic technique.

1. Introduction

The competition between the antiferro- and ferro-electric interactions among the adjacent smectic layers in chiral tilted smectic liquid crystals causes an appearance of different ferro-, ferri- and antiferro-electric phases [1, 2]. A detailed study of the relaxation processes has been made using dielectric spectroscopy [3–10], electro-optics [7, 8, 10] and photon correlation spectroscopy [11]. However the previous dielectric measurements were made over a limited range of frequencies of up to only 10 MHz. Some of the results are not understood and in some cases the assignments contradict each other. The problem of finding the mechanisms governing the various relaxation processes in the antiferroelectric phase has not yet been solved and the aim of this paper is to establish these mechanisms unambiguously. The main purpose of this work is the theoretical and experimental investigation of the relaxation processes in the antiferroelectric SmC_A phase using dielectric (up to 1 GHz) and electro-optic spectroscopy (up to 100 kHz) of an AFLC sample over a wider range of frequencies. These studies are carried out with a view to establishing the origin of the various relaxation processes. Due to the absence of a net spontaneous polarization in the SmC_A phase, dielectric loss is found to be much lower compared with that in the ferri- and ferro-electric phases. Furthermore, the magnitude of the dielectric loss for the collective relaxation modes is comparable to that of the molecular relaxation modes. Although the nature of the relaxation process in the SmC_A phase has been somewhat speculated over in earlier publications [5–9], nevertheless no clear evidence is provided and no theoretical investigations have so far been made. The mechanism of the collective processes is found by comparing the results of dielectric and electro-optic spectroscopy with those from theoretical investigations. The experimental and theoretical aspects for the observation of the distortion of an antiferroelectric helix through polar and dielectric anisotropy interactions, outlined in [17], are detailed.

*Author for correspondence.

2. Experimental

We investigated the dynamics of an antiferroelectric liquid crystalline material with and without bias voltage for cells of thicknesses varying from 8 to 100 μm. The AFLC sample used in experiments was AS-573 (University of Hull, U.K) with the following phase transition sequence (provided by conoscopy and spontaneous polarization measurements) [10, 12]:

$$SmC_A\ 78\ SmC_\gamma\ 81\ AF\ 83\ FiLC\ 90\ SmC^*\ 93\ SmA\ 106\ I\ (^\circ C)$$

where AF and FiLC represent further phases with antiferroelectric and ferrielectric characteristics, respectively.

For the dielectric measurements made at frequencies below 10 MHz, the sample cell consisted of ITO coated

glass plates with a low resistance of 30 Ω/□. The cells for high frequency measurements (>1 MHz) were prepared using gold-coated brass electrodes. For planar alignment, the conducting inner surfaces were spin-coated with a PVA alignment layer and rubbed parallel. The cells were first filled with the liquid crystal in the isotropic phase. Textures of the material in experimental cells were observed using polarizing optical microscopy. Dielectric measurements in the frequency range 1 Hz to 100 kHz were made using a Schlumberger 1255A frequency response analyser (FRA) with the sample connected to the FRA through a Chelsea dielectric interface. For measurements at higher frequencies, Hewlett Packard impedance analysers HP-4192A (10 kHz–10 MHz) and HP-4191A (10 MHz–1 GHz) were used. The experimental systems enabled the superimposition of d.c. bias voltages up to 40 V on an alternating measuring voltage of 0·05 V_{rms} applied across the sample. The accuracy of measurements of ε' and ε'' within the entire frequency range is within $\pm 2\%$ and $\pm 5\%$, respectively. The dielectric response of multidomain cell can be different from a monodomain cell, especially for measuring voltages greater than 0·2 V_{rms} due to the switching of domains. This is not so in the antiferroelectric phase since the spontaneous polarization is zero. In any case, the measuring voltage in dielectric experiments is much lower than 0·2 V_{rms}. Homeotropic alignment was produced using carboxylatochromium complexes (chromolane) as the aligning agent, but electrodes were not rubbed. The smectic layers in a homeotropic cell are considered to be parallel to the electrodes. This was confirmed by polarization microscopy, when the cell in the SmA phase was dark due to the molecules being parallel to the direction of incidence of the light. The homeotropic alignment was used for making some of the high frequency dielectric measurements in order just to confirm the temperature dependence of the relaxation frequency of the molecular relaxation process around the short axis. The relaxation processes other than the rotation around the short axis are suppressed in the homeotropic alignment.

The complex dielectric permittivity $\varepsilon(\omega)$, measured for a homogeneous alignment of the AFLC sample is fitted to the Havriliak–Negami (HN) equation [18]

$$\varepsilon(\omega) - \varepsilon_\infty = \sum_{i=1}^{n=4} \frac{\Delta\varepsilon_i}{[1 + (i\omega\tau_i)^{\alpha_i}]^{\beta_i}} - \frac{i\sigma}{\varepsilon_0 \omega^s} \qquad (1)$$

where σ is the specific conductivity, s is a fitting parameter of the conductivity term $0{\cdot}5 < s \leqslant 1$ and ω is the angular frequency. The relaxation strength $\Delta\varepsilon_i$, the relaxation frequency ($f_{mi} = 1/2\pi\tau_i$), and the distribution parameters (α_i and β_i) of the relaxation processes are obtained by fitting the data to the HN equation, where n is the number of processes for some temperatures, for some phases, $n = 4$ and for others 3. If $\alpha_i \neq 1$ and $\beta_i \neq 1$, f_{mi} is different from the frequency of the loss maximum. However, both of these parameters were found to be close to unity. The computer program finds the mean deviation of the dielectric loss (calculated from the fitted parameters) from the measured values, minimizes it and finds the optimum parameters, and also displays the fitted curve relative to the experimental curve. A representative fitting of the data at a temperature of 70°C to four loss curves and a term due to the conductivity is shown in figure 1 (*a*). This appears to be a good fitting between the experimental and the calculated curves. The inputs to the program are the first approximations to these parameters; these are guessed in the first instance from

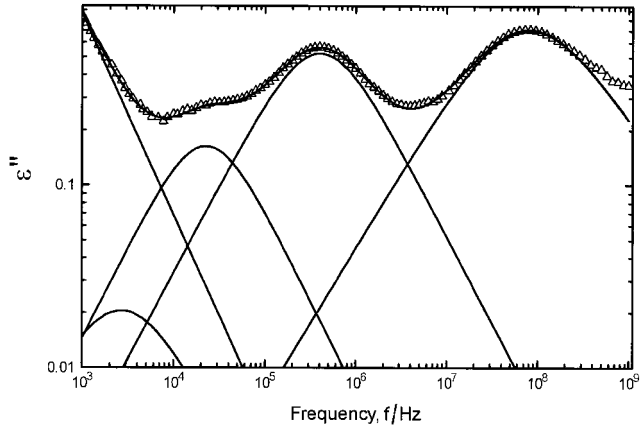

(*a*)

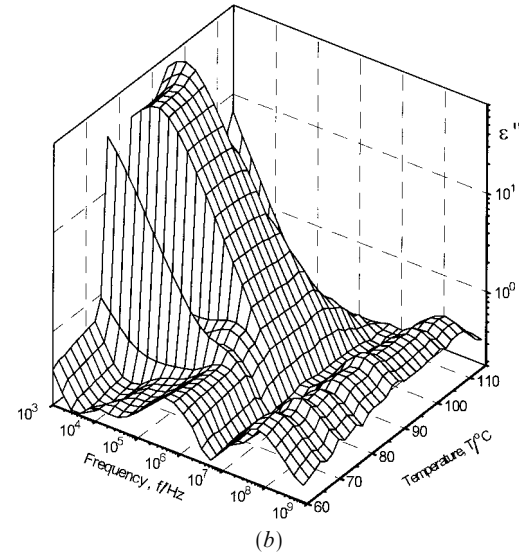

(*b*)

Figure 1. (*a*) The fitting at 70°C in the SmC_A phase to four relaxation processes and a conductivity process. (*b*) Dielectric loss spectra for AS-573, $d = 50\,\mu m$, versus frequency and temperature.

the loss curves. An accuracy of estimation of these parameters is well within $\pm 10\%$.

For electro-optic spectroscopy, a lock-in amplifier with a facility to lock the amplifier to both the fundamental and the second harmonic frequency of the signal applied across the sample, has been used. In this technique, the sample is modulated by a weak alternating field and the transmittances at the fundamental and second harmonic of the applied field were measured. For investigating the linear frequency modes, almost perfectly homogeneously aligned cells were used. For measurements at the second harmonic frequency, non-aligned cells were employed in order to suppress the signal at the fundamental mode. The relaxation frequency is defined as the frequency where the phase difference relative to the low frequency response is 90°. This definition is similar to that given by Hiraoka *et al.* [8].

3. Results and discussion

Figure 1 (*b*) shows the dielectric loss (ε'') spectra in the frequency range $10^3 - 10^9$ Hz for the temperature range from 60°C to 115°C, and also shows the existence of the various phases in this sample: SmC_A, SmC_γ, AF, FiLC, SmC*, SmA, I. In the SmC_A phase at 70°C, we find three peaks centred at approximately 10 kHz, 300 kHz and 60 MHz. At a temperature of 82°C in the AF phase, we also find three peaks. In the isotropic phase at 110°C, again two peaks are seen, these being centred at 5 MHz and 280 MHz. Figure 1 (*a*) shows fitting of the experimental curve to the Havriliak–Negami equation. Figures 2 and 3 show the temperature dependence of the dielectric parameters of the material: these were found by fitting the dielectric spectra for different temperatures such as is shown in figure 1 (*a*).

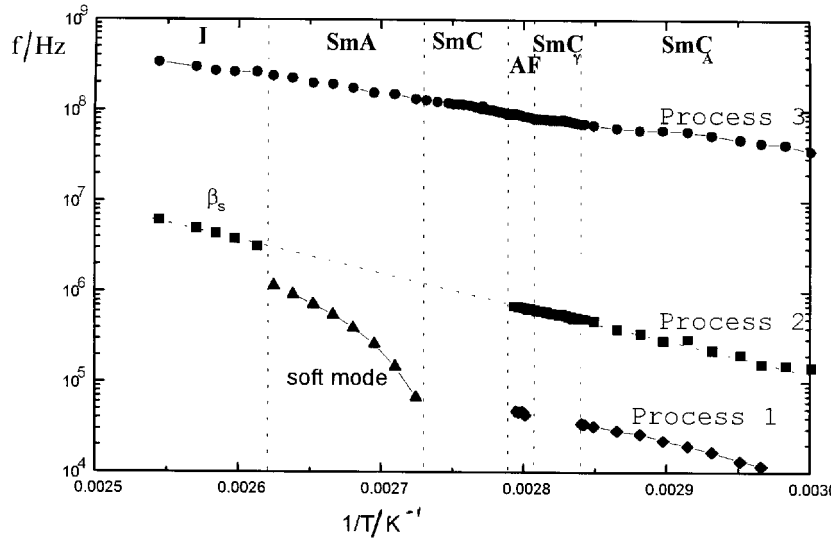

Figure 2. Dependence of the relaxation frequency (f) on inverse temperature for AS-573, $d = 50\,\mu$m: ◆ (AF) antiferroelectric relaxation Process 1, ■ (β_S) beta relaxation around the molecular short axis, ● (β_1) beta relaxation around the molecular long axis, ▲ soft mode.

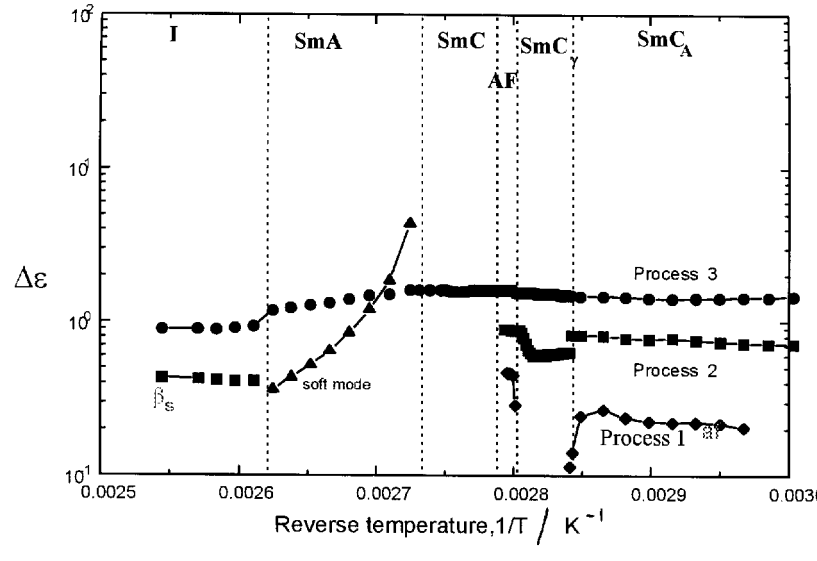

Figure 3. Dependence of the dielectric strength ($\Delta\varepsilon$) on inverse temperature for AS-573, $d = 50\,\mu$m: ◆ (AF) antiferroelectric relaxation Process 1, ■ (β_S) beta relaxation around the molecular short axis, ● (β_1) beta relaxation around the molecular long axis, ▲ soft mode.

The relaxation processes observed in the SmA, SmC*, FiLC and SmC_γ phases have been discussed in a previous paper [10]; the discussion here is specifically limited to the processes observed in the antiferroelectric phase. In the above figures, we show three relaxation processes in the SmC_A phase and these are denoted as Processes 1, 2, 3 with increasing frequency. The lowest frequency Process 0, with a relaxation frequency of $\sim$2·5 kHz had been reported to exist under the bias voltage at frequencies up to 10 MHz by Hiller *et al.* [5] and Hiraoka *et al.* [8] and also in the absence of bias voltage by Buivydas *et al.* [6]. In our investigations, this process was also found to exist even without the bias voltage; however, due to its reduced dielectric strength and lower relaxation frequency, it is considerably superimposed by the dielectric loss arising from the ionic conductivity. It could however be detected by a fitting procedure that was carried out by subtracting contributions from the ionic conductivity. Nevertheless in the absence of the bias voltage, the dielectric parameters for this process at various temperatures contain large errors for the reasons already given and therefore they are not shown in figures 2 and 3. The application of bias voltage enhances the dielectric strength of Process 0 (the reason will be given later) and also reduces the effect of the ionic conductivity by drawing the charge carriers to the electrodes. The dielectric parameters found from the fitting procedure under bias voltage become more reliable and are presented and discussed later in this paper.

3.1. *Molecular relaxation processes*

For temperatures corresponding to the isotropic phase, two molecular relaxation processes are observed (figures 2 and 3). The higher frequency process is tentatively assigned to a rotation around the molecular long axis [13, 14] (β_l), and the lower frequency process to that around the molecular short axis [4, 13] (β_s). The reasons for the assignment are given below. The activation energy for the molecular relaxation process around the short axis ($\approx$68 kJ mol^{-1}) is greater than that for the long axis ($\approx$40 kJ mol^{-1}), as normally expected [13]. Investigations of the molecular relaxation processes show that the temperature dependence of the relaxation frequency follows the Arrhenius law. The activation energy is reported to be independent [4, 13] or slightly dependent [14] on the type of liquid crystalline mesophase and the relaxation frequencies have no discontinuities or jumps at the phase transition temperatures.

The molecular relaxation process around the long axis can easily be observed over a wider temperature range because of its high value of the relaxation frequency. The dependence of the relaxation frequency of this process on temperature is governed by the Arrhenius law over the intermediate liquid crystalline phases. Process 3 in the antiferroelectric phase can therefore be unambiguously assigned to molecular rotation around the long axis.

The mechanism of the relaxation Process 2 is not so obviously clear. The magnitude of the relaxation strength and the frequency of the molecular relaxation process around the molecular short axis are relatively low, and the process is also screened by the dominant Goldstone mode in the SmC* and SmC_γ phases. However, the temperature dependence of the frequency of Process 2 in the antiferroelectric phases can be extrapolated to that around the molecular short axis in the isotropic phase as shown in figure 2. Finally, in order to confirm the assignment for this mode, we also carried out dielectric measurements over wide ranges of temperature and frequency for the homeotropically aligned cells. For such aligned cells, the collective relaxation processes are suppressed and the temperature dependence of the dielectric parameters for the molecular relaxation processes are found over the entire temperature range [4, 8]. The relaxation frequency continuously decreases with decrease in the temperature according to the Arrhenius law and is found to have the same value as the frequency for Process 2 in the antiferroelectric SmC_A phase. A comparison of the relaxation frequencies for homogeneously and homeotropically aligned cells leads us finally to conclude that Process 2 in the SmC_A phase is caused by molecular rotation around the short axis. We have already established that Process 3 arises from rotation around the long axis.

3.2. *Collective relaxation processes in the antiferroelectric phase*

The lower frequency processes (Process 0 and Process 1) are found to exist only in the two antiferroelectric phases SmC_A and AF phases. The frequency of Process 0 is $\sim$2·5 kHz, whereas that of Process 1 lies between 10 and 70 kHz depending on the temperature. Hence it can only be concluded that these processes are specifically related to the common characteristics of antiferroelectric phases. The origin of these processes is still to be explained. Four possible physical mechanisms, some of these already suggested [4–6, 8, 9] for collective molecular reorientations, in the antiferroelectric phase are schematically presented in figure 4 and described as follows.

(i) A deviation from the antiferroelectric order by the azimuthal angle φ, such that φ changes in the opposite sense [8] in adjacent layers [figure 4 (*a*)]. The mode concerning the fluctuation in φ of the type shown in figure 4 (*a*) in the antiferroelectric phase was called the antiferroelectric Goldstone

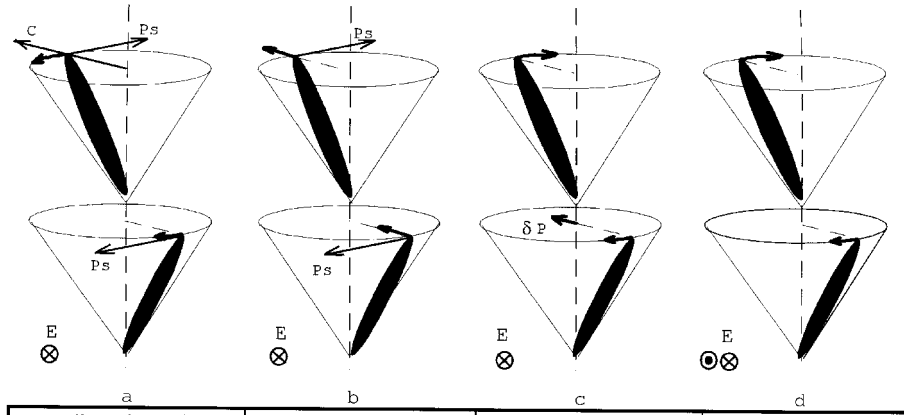

distortion of antiferroelectric order	electroclinic (soft mode)	helix distortion due to antiferroelectric polarization	helix distortion due to dielectric anisotropy
polar	polar	polar	non-polar
$\alpha(E)\neq 0$	$\alpha(E)\neq 0$	$\alpha(E)=0$	$\alpha(E)=0$
	DIELECTRIC	SPECTRA	
Process 1 (20 kHz)	not detected	Process 0 (2.5-3 kHz)	not detected
	ELECTROOPTIC	SPECTRA	
single frequency response (20kHz)	not detected	not detected	double frequency response (6 kHz)
Hiraoka et al. *Ferroelectrics*, **147**, 13 (1993).	Hiraoka et al. *Ferroelectrics*, **147**, 13 (1993).	M.Buivydas et al. *Liq.Cryst.*, **18** (6), 879 (1995).	Panarin et al. *Appl. Phys. Lett.*, **72**, 1667 (1998).
(a)	**(b)**	**(c)**	**(d)**

Figure 4. Four different physical mechanisms for the molecular rearrangements in the antiferroelectric SmC_A phase under the applied voltage. $\mathbf{P}_s$ is the spontaneous polarization vector, C being the C-director.

mode by Hiraoka *et al.* [8]. However, a change of φ in the opposite sense for two adjacent layers, due to rotations of the directors in the opposite directions, is termed 'the anti-phase motion' by Buivydas *et al.* [6]. The terminology 'anti-phase motion', or distortion of the antiferroelectric order caused by the anti-phase motion, is more appropriate for the reason that it depicts the mechanism more clearly. The antiferroelectric Goldstone mode in our view is considered more appropriate for another relaxation process [figure 4 (*c*)], the mechanism of which is similar to that of a ferroelectric Goldstone mode.

(ii) Fluctuations in the tilt angle (θ) or the antiferroelectric soft mode as depicted in figure 4 (*b*).

(iii) Helical Goldstone mode due to the existence of 'antiferroelectric' polarization $\delta\mathbf{P}$, as shown in figure 4 (*c*); also see figure 5. The explanations for the antiferroelectric polarization are given below.

(iv) A disturbance of the antiferroelectric helix due to the dielectric anisotropy, $\Delta\varepsilon\mathbf{E}^2$, figure 4 (*d*).

3.2.1. *Origin of Process 0*

The C-directors in adjacent smectic layers are not completely antiparallel to each other even in the anti-

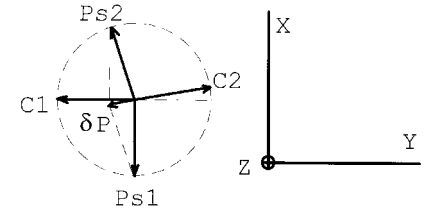

Figure 5. Schematic presentation of the arrangement of the C-directors ($C1$, $C2$) and the local spontaneous polarization ($\mathbf{P}_s1$, $\mathbf{P}_s2$) of two neighbouring smectic layers in the helical antiferroelectric phase with respect to the laboratory frame of reference.

ferroelectric phases as has already been suggested by Buivydas *et al.* [6]. This will give rise to the 'antiferroelectric spontaneous polarization' $\delta\mathbf{P}$ as shown in figure 4 (*c*). This is found to be almost parallel to the C-directors and is shown in figure 5. It is possible to estimate the value of such an 'antiferroelectric polarization' $\delta\mathbf{P}$. Taking into account the typical value of the helical pitch $\approx$2000 Å and the smectic layer thickness $\approx$40 Å, a trivial calculation shows that the angle between the spontaneous polarization vectors in two adjacent smectic layers is approximately 176–177 degrees and the value of the 'antiferroelectric polarization' $\delta\mathbf{P}$ is approximately

3% of that of the spontaneous polarization $\mathbf{P}_s$. Such an 'antiferroelectric polarization' should spiral along the helical axis as the polarization does in a ferroelectric phase. Hence we can expect the dielectric relaxation process to arise from the distortion of the antiferroelectric helix similarly to the cause of a ferroelectric helical Goldstone mode.

The relaxation Process 0 is then an antiferroelectric helical Goldstone mode that arises from the interaction of the 'antiferroelectric' polarization with the electric field. The dependence of $\Delta\varepsilon$ on the bias voltage for the relaxation Process 0 is shown in figure 6. $\Delta\varepsilon$ first increases rapidly and then decreases gradually with the bias voltage. Buivydas *et al.* [6] detected this mode in an AFLC mixture having a low temperature SmC_A phase of almost negligible ionic conductivity. The latter is probably the reason why Buivydas *et al.* [6] could detect this mode even in the absence of the bias voltage, while other investigators [5, 8] could not observe it since in their samples this mode was screened by the ionic conductivity. The increase of $\Delta\varepsilon$ with bias voltage could be explained in terms of $\delta\mathbf{P}$ increasing with the bias voltage. $\delta\mathbf{P}$ in the first instance arises from the distortion of the antiferroelectric order [due to the process pointed out in figure 4 (*a*)]; an increase in the non-compensated polarization is brought about by the bias voltage. The mechanism of this mode under weak field is then governed by the in-phase motion as depicted in figure 4 (*c*); this mode arises from the distortion of the helix. The reason for the eventual decrease of $\Delta\varepsilon$ with bias voltage is that the antiferroelectric helix is first highly distorted and then eventually unwound for higher bias voltages. To clarify further and confirm the physical mechanism for Process 0, we have made a theoretical study of the relaxation processes of the antiferroelectric helix. We have also carried out electro-optic spectroscopic investigations of the sample in the SmC_A phase.

3.2.2. *Origin of Process 1*

The relaxation frequency of Process 1 is higher than that of Process 0. The mechanism can either be the anti-phase motion of the type shown in figure 4 (*a*) or soft mode, figure 4 (*b*). Hiraoka *et al.* [8] suggested an 'antiferroelectric-like' Goldstone mode for this type of motion. We may point out however that this is a misleading terminology as the antiferroelectric Goldstone mode should be reserved for Process 0 due to its similarity to that of a ferroelectric Goldstone mode, as mentioned above. In certain investigations [4] of samples having a direct SmC_A–SmA transition, this process was also assigned to the soft mode mainly because it followed a typical behaviour for this mode close to the transition temperature, i.e. the relaxation frequency increased with temperature on either side of the transition. Nevertheless, 20°C below this temperature the relaxation frequency was found to decrease with decreasing temperature. Similar behaviour is also seen in figure 3 for the sample under investigation here. Although a decrease in the relaxation frequency can be explained by an increase in the rotational viscosity with decreasing temperature, nevertheless an unusual dependence of $\Delta\varepsilon$ such as that observed in figure 3 has no proper explanation, i.e. $\Delta\varepsilon$ decreasing instead of increasing close to the transition temperature. Therefore we rule out the 'antiferroelectric soft mode' as a possible physical mechanism for the process 1. the relaxation Process 1 is therefore tentatively assigned to the distortion of the antiferroelectric order [8] caused by the anti-phase motion [figure 4 (*a*)] and the mode should be so called. This mechanism will be confirmed through electro-optic spectroscopic investigations.

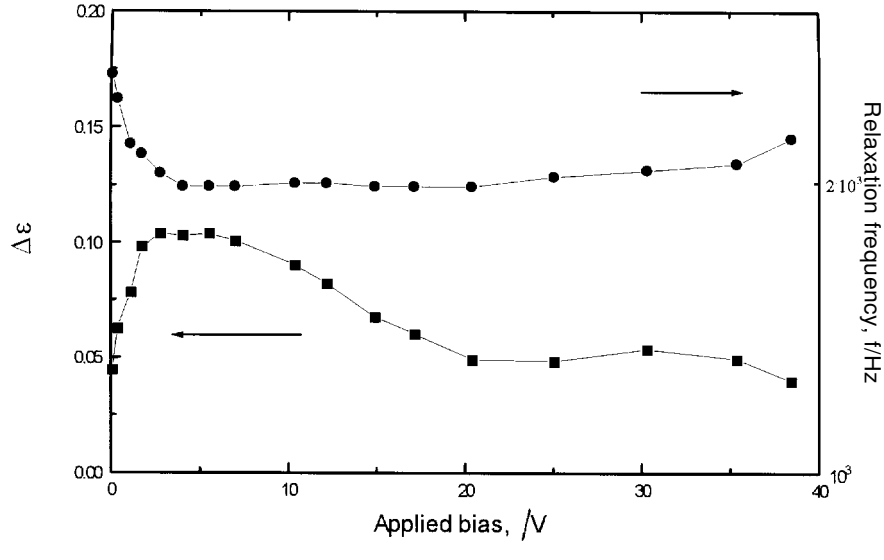

Figure 6. The dependence of the dielectric parameters ($\Delta\varepsilon$) and the relaxation frequency (f) of the lowest frequency relaxation process (Process 0) on bias voltage.

However, in the literature no direct evidence for the mechanism has been given.

3.3. *A theoretical study of the relaxation processes due to the antiferroelectric helix*

Consider the antiferroelectric liquid crystal cell (AFLC) in bookshelf geometry as shown in figure 7. On assuming the existence of the antiferroelectric polarization $\delta\mathbf{P}$, the equation for the director motion in the antiferroelectric phase can be written as follows:

$$\gamma_\varphi \sin^2\theta \frac{\partial\varphi}{\partial t} = K_\varphi \sin^2\theta \frac{\partial^2\varphi}{\partial z^2} + \delta\mathbf{P}\mathbf{E}\cos\varphi + \frac{\Delta\varepsilon}{4\pi}\mathbf{E}^2 \sin^2\theta \sin\varphi\cos\varphi \qquad (2)$$

where γ_φ is the rotational viscosity, K_φ the elastic constant, θ the molecular tilt angle, φ the azimuthal angle and $\Delta\varepsilon$ the dielectric anisotropy. The torque due to polar interactions is $\delta\mathbf{P}\mathbf{E}\cos\varphi$ due to the fact that $\delta\mathbf{P}$ is almost perpendicular to the spontaneous polarization $\mathbf{P}_s$.

On using the formula $\cos\varphi\sin\varphi = \sin(2\varphi)/2$, and on changing variables such that

$$\gamma = \gamma_\varphi \sin^2\theta, \quad K = K_\varphi \sin^2\theta \quad \text{and} \quad \Delta\varepsilon^* = \frac{\Delta\varepsilon \sin^2\theta}{8\pi} \qquad (3)$$

we get

$$\gamma\frac{\partial\varphi}{\partial t} = K\frac{\partial^2\varphi}{\partial z^2} + \delta\mathbf{P}\mathbf{E}\cos\varphi + \Delta\varepsilon^*\mathbf{E}^2\sin 2\varphi. \qquad (4)$$

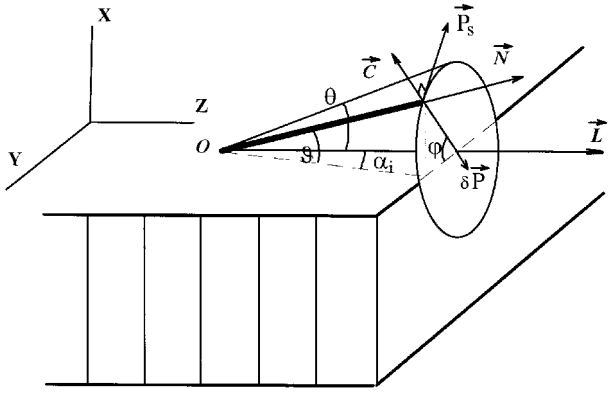

Figure 7. Smectic layer structure for a bookshelf cell. (X, Y, Z) is the co-ordinate system, N is the molecular director, L the smectic layer normal, C the C-director, θ the tilt angle, ϑ the angle between the molecular director and the electrode plane, φ the azimuthal angle and α_i the angle between the smectic layer normal and the projection of the molecular directors on the plane of the electrodes.

For the electric field $\mathbf{E}(t) = \mathbf{E}_0\cos\omega t$, equation (4) takes the form:

$$\gamma\frac{\partial\varphi}{\partial t} = K\frac{\partial^2\varphi}{\partial z^2} + \delta\mathbf{P}\mathbf{E}_0\cos\omega t\cos\varphi + \Delta\varepsilon^*\mathbf{E}_0^2\cos^2\omega t\sin 2\varphi. \qquad (5)$$

Equation (5) can be written as:

$$\gamma\frac{\partial\varphi}{\partial t} = K\frac{\partial^2\varphi}{\partial z^2} + \delta\mathbf{P}\mathbf{E}_0\cos\omega t\cos\varphi + \frac{\Delta\varepsilon^*}{2}\mathbf{E}_0^2[\cos(2\omega t)+1]\sin 2\varphi \qquad (6)$$

or

$$\gamma\frac{\partial\varphi}{\partial t} = K\frac{\partial^2\varphi}{\partial z^2} + \delta\mathbf{P}\mathbf{E}_0\exp(\mathrm{j}\omega t)\cos(\varphi) + \frac{\Delta\varepsilon^*}{2}\mathbf{E}_0^2[\exp(\mathrm{j}2\omega t)+1]\sin(2\varphi). \qquad (7)$$

Assuming $\mathbf{E}_0$ is sufficiently small, and applying the standard perturbation technique, let the solution be of the following form:

$$\begin{aligned}\varphi(z,t) &= qz + f(z,t)\\ &= qz + \cos(qz)[f_{12}\exp(\mathrm{j}2\omega t) + f_{11}\exp(\mathrm{j}\omega t) + f_{10}]\\ &\quad + \sin(2qz)[f_{22}\exp(\mathrm{j}2\omega t) + f_{21}\exp(\mathrm{j}\omega\tau) + f_{20}]\end{aligned} \qquad (8)$$

where f_{10}, f_{11}, f_{21} and f_{20}, f_{12}, f_{22} are the coefficients of a Fourier series proportional to $\mathbf{E}_0$ and $\mathbf{E}_0^2$. On substituting equation (8) into (7), we find the following algebraic equation:

$$\begin{aligned}&\mathrm{j}\omega\gamma\cos(qz)[f_{11}\exp(\mathrm{j}\omega t) + 2f_{12}\exp(\mathrm{j}2\omega t)]\\ &\quad + \mathrm{j}\omega\gamma\sin(2qz)[f_{21}\exp(\mathrm{j}\omega t) + 2f_{22}\exp(\mathrm{j}2\omega t)]\\ &= -Kq^2\cos(qz)[f_{11}\exp(\mathrm{j}\omega t) + f_{12}\exp(\mathrm{j}2\omega t) + f_{10}]\\ &\quad - 4Kq^2\sin(2qz)[f_{22}\exp(\mathrm{j}2\omega t)\\ &\quad + f_{21}\exp(\mathrm{j}\omega t) + f_{20}] + \delta\mathbf{P}\mathbf{E}_0\exp(\mathrm{j}\omega t)\cos(qz)\\ &\quad + \frac{\Delta\varepsilon^*}{2}\mathbf{E}_0^2[\exp(\mathrm{j}2\omega t)+1]\sin(2qz).\end{aligned} \qquad (9)$$

This equation consists of terms in single frequency, terms in double frequency and terms independent of frequency. Hence equation (9) can be separated by equating terms of the same frequency. This leads to a set of the following

six equations:

$$j\omega\gamma f_{11}\cos(qz)\exp(j\omega t) = -Kq^2 f_{11}\cos(qz)\exp(j\omega t) + \delta\mathbf{P}\mathbf{E}_0\exp(j\omega t)\cos(qz) \quad (10)$$

$$2j\omega\gamma\sin(2qz)f_{22}\exp(j2\omega t) = -4Kq^2\sin(2qz)f_{22}\exp(j2\omega t) + \frac{\Delta\varepsilon^*}{2}\mathbf{E}_0^2\exp(j2\omega t)\sin(2qz) \quad (11)$$

$$0 = -4Kq^2\sin(2qz)f_0 + \frac{\Delta\varepsilon^*}{2}\mathbf{E}_0^2\sin(2qz) \quad (12)$$

$$j2\omega\gamma f_{12}\cos(qz)\exp(j2\omega t) = -Kq^2 f_{12}\cos(qz)\exp(j2\omega t) \quad (13)$$

$$j\omega\gamma f_{21}\sin(2qz)\exp(j\omega t) = -4Kq^2\sin(2qz)f_{21}\exp(j\omega t) \quad (14)$$

$$0 = q^2 f_{10}\cos(qz). \quad (15)$$

On solving equations (10)–(12), we find the coefficients f_{11}, f_{22} and f_{20}:

$$f_{11} = \frac{\delta\mathbf{P}\mathbf{E}_0}{Kq^2}\frac{1}{(j\omega\tau_1+1)}, \quad \text{where} \quad \tau_1 = \frac{\gamma}{Kq^2} \quad (16)$$

$$f_{22} = \frac{\Delta\varepsilon^*\mathbf{E}_0^2}{8Kq^2}\frac{1}{(j\omega\tau_2+1)}, \quad \text{where} \quad \tau_2 = \frac{\gamma}{2Kq^2} \quad (17)$$

and

$$f_{20} = \frac{\Delta\varepsilon^*\mathbf{E}_0^2}{8Kq^2}. \quad (18)$$

Equations (13)–(15) are valid only when the coefficients f_{12}, f_{21} and f_{10} are equal to zero.

The most important aspect of the solution is the existence of the two types of helical distortions caused by the applied electric field. These are explained diagramatically. Figure 8 shows the distribution of the C-directors along the helical axis in the antiferroelectric phase. The C-directors of two adjacent layers are almost antiparallel and are shown together. The application of the electric field will cause a distortion of the helix (azimuthal angle φ) due to the two different mechanisms of interaction ($\delta\mathbf{P}\mathbf{E}$ and $\Delta\varepsilon\mathbf{E}^2$) in two different ways shown in figure 8. The solid line is the distribution of the azimuthal angle φ along an undisturbed helix, the dotted line shows the distortion of the helix due to the polar interactions ($\delta\mathbf{P}\mathbf{E}$) and the dashed line shows that due to the interactions with the field arising from dielectric anisotropy ($\Delta\varepsilon\mathbf{E}^2$).

The frequency dependence of the coefficient f_{11} for the polar process, equation (16), is the same as that for the usual helical Goldstone mode in FLCs [13]. The dynamic properties of the helical distortion mode in the ferroelectric phase have been investigated by Levstik *et al.* [15]. They derived the following expressions for the dielectric relaxation parameters:

$$\Delta\varepsilon = \frac{\mathbf{P}_s^2}{2\varepsilon_0 K_\varphi \sin^2\theta\, q^2} \qquad \tau = \frac{\gamma_\varphi}{K_\varphi q^2}. \quad (19)$$

Hence, on comparing equations (16) and (19), we find that the dielectric strength of the antiferroelectric Goldstone mode is ≈1000 times (3%) smaller than the dielectric strength of the ferroelectric Goldstone mode. This is in good agreement with the experimental results where the dielectric strength of the ferroelectric Goldstone mode

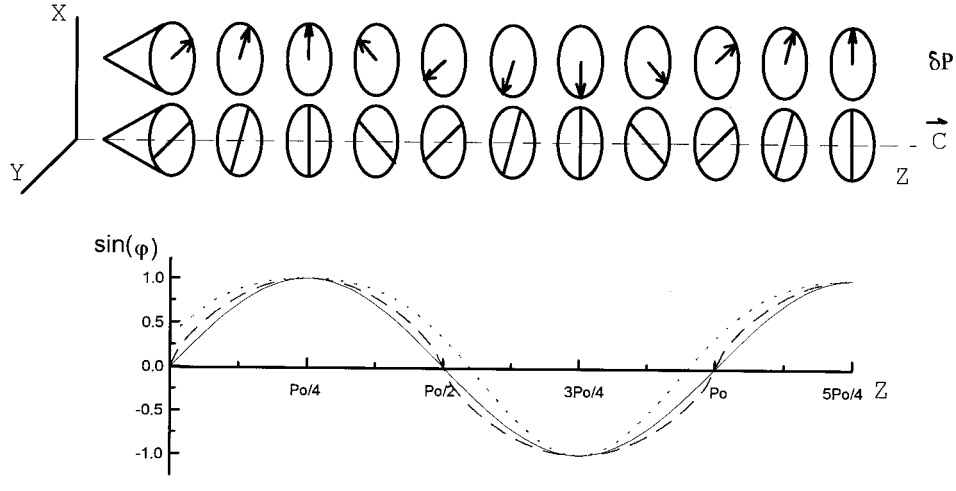

Figure 8. Schematic arrangement (upper part) of the antiferroelectric polarization $\delta\mathbf{P}$ and the C-director along the Z-axis and (lower part) the distortion of the helix due to the polar interactions, $\delta\mathbf{P}\mathbf{E}$ (dotted line), and those due to the dielectric anisotropy, $\Delta\varepsilon\mathbf{E}^2$ (dashed line).

is of the order of 70–80 [10] and the dielectric strength of the antiferroelectric Goldstone mode for Process 0 shown in figure 6 is 0·5–0·6.

In the usual ferroelectric helical system, the double frequency relaxation process arising from the dielectric anisotropy is also predicted, but the amplitude of this process will be much lower than the amplitude of the polar relaxation process.

It follows from the solution of equation (2), given in equations (16) and (17), that the relaxation time of the polar helical distortion mode τ_1 is double the relaxation time due to the dielectric anisotropy τ_2. In other words the relaxation frequency of Process 0 due to the distortion of the helix caused by the polar interactions is half the distortion caused by the dielectric anisotropy. Although a non-polar relaxation process (i.e. caused by dielectric anistropy) could not be detected by dielectric relaxation spectroscopy, it can be investigated by electro-optic spectroscopy.

3.4. *Electro-optic spectroscopy*

The transmittance of a FLC between crossed polarizers can be expressed by the formula:

$$T = \sin^2[2(\beta+\alpha)]\sin^2\left(\frac{\pi\Delta n d}{\lambda}\right) \qquad (20)$$

where β is the angle between the smectic layer normal and the polarizer axis, α is the angle between the smectic layer normal and the average projection of the molecular directors on the plane of the electrodes, Δn is the effective (average) birefringence, λ is the light wavelength and d is the cell thickness.

Let us now consider the electro-optic response to be due to four possible mechanisms as shown in figure 4, where for different modes, the motion of the directors in two adjacent layers is shown. Since the distance between the two neighbouring smectic layers is much smaller than the wavelength of the light beam, we can consider the average angle α for the two neighbouring smectic layers as $\alpha = (\alpha_1 + \alpha_2)/2$, where α_i with $i = 1$ or 2 is the angle between the layer normal and the projection of the molecular director of the ith smectic layer on the plane of the electrodes (figure 7). For the antiferroelectric phase and in the absence of the electric field, the average angle α between the smectic layer normal and the projection of the molecular directors on the plane of the electrodes is equal to zero since $\alpha_1 = -\alpha_2$. Application of the electric field can cause the reorientation of molecules by one or up to four possible mechanisms. The change in the azimuthal angle, φ (i.e. between the Y-axis and the C-director, or between the X-axis and $\mathbf{P}_s$) due to the polar interactions **PE** [figure 4 (*a*)] will make the angle $\alpha \neq 0$. This is because the directors are moving in the opposite sense in adjacent layers or in anti-phase, i.e. one moving clockwise and the other anticlockwise. For $\mathbf{E} \neq 0$, $|\alpha_1| > |\alpha_2|$ if the mechanism as depicted in figure 4 (*a*), the distortion of antiferroelectric order (anti-phase $\rightarrow$ antiferroelectric Goldstone mode) is followed. The sign of α_i depends on the polarity of the field. The intensity of the transmitted light and the frequency of the electro-optical response due to this interaction depend on the initial angle β between the smectic layer normal and the polarizer axis. According to equation (1), one can show that the electro-optical response will be of the same frequency as the applied voltage for values of β lying in the range $\alpha < \beta < 45 - \alpha$ and of double the frequency for $\beta = 0°$ and 45°. So choosing $\beta = 22{\cdot}5°$ we can guarantee the condition for the electro-optic response to exist at the fundamental frequency. The same will also be valid for the reorientational mechanism caused by the antiferroelectric soft mode, figure 4 (*b*). The experiment for this part of the electro-optic spectroscopy is therefore carried out by having $\beta = 22{\cdot}5°$.

A different type of electro-optic response should be observed if the mechanism for the electrostatic interaction $\Delta\varepsilon\mathbf{E}^2$ through dielectric anisotropy were valid for these phases. In this case the directors of the two adjacent smectic layers move in the opposite sense to the field direction. The average angle α_i will always be equal to 0 and independent of the field; on application of the field the magnitude of the angle α in both layers would be the same. The electro-optical response in this case will only be due to the second term in equation (2), namely that due to the change in the effective birefringence Δn, and will always be of the double frequency because of the sine-squared term. The effective birefringence Δn_{eff} depends on the angle ϑ between the molecular director and the plane of the electrodes through the following equation [16]:

$$\Delta n_{\text{eff}} = n_Z - n_Y = \frac{n_\parallel n_\perp}{[n_\parallel^2 \sin^2(\vartheta) + n_\perp^2 \cos^2(\vartheta)]^{1/2}} - n_\perp \qquad (21)$$

where n_Z and n_Y are the refractive indices of the light beam propagating in the X-direction for the electric vectors distributed in the Z- and Y-directions, respectively. The application of the electric field will reorientate the molecules on a cone so as to increase the angle ϑ and thus decrease the effective birefringence Δn_{eff}. The angle ϑ is related to φ through the following equation (figure 5)

$$\tan\vartheta = \tan\theta\sin\varphi \qquad (22)$$

or for small θ,

$$\vartheta \approx \theta\sin\varphi. \qquad (23)$$

The birefringence in the refractive index will therefore be modulated by the field. Values of ϑ and Δn_{eff} however do not depend on the sign of the electric field; therefore we can expect the electro-optic response due to this interaction be of twice the frequency of the applied field. This response due to the birefringence in the refractive index would also be superimposed for the cases presented in figures 4 (*a*) and 4 (*b*). However in these cases, it could be neglected by selecting a single frequency measuring mode on the lock-in amplifier as the response due to the induced α would be much greater than that due to the birefringence in the refractive index.

The electro-optic measurements were carried out on a cell with 20 μm thick sample at a temperature of $T = 75$°C. It has been found that for well homogeneously aligned cells, the response per unit volt or the linear response due to a change in the angle α is much greater than the quadratic response arising from a change in the effective birefringence. Figure 9 presents the dependence of the intensity per unit volt (I/V) of the linear and double frequency responses on the applied voltage (V). As expected from the solution of equation (2), the amplitude of the single frequency response is linearly dependent on applied voltage, while the double frequency response is quadratically dependent on voltage for sufficiently small values ($V < 10$ V). For higher voltages, the response falls and this can be explained by taking terms of $\mathbf{E}_0^3$ and higher in equation (8).

Figure 10 shows the dependence of the amplitude part and the phase part of the electro-optic response at the same frequency as the applied signal for an almost perfectly homogeneously aligned cell. The relaxation frequency is found to be approximately 20–30 kHz and is almost of the same magnitude as for the dielectric relaxation Process 1. Therefore we can unambiguously

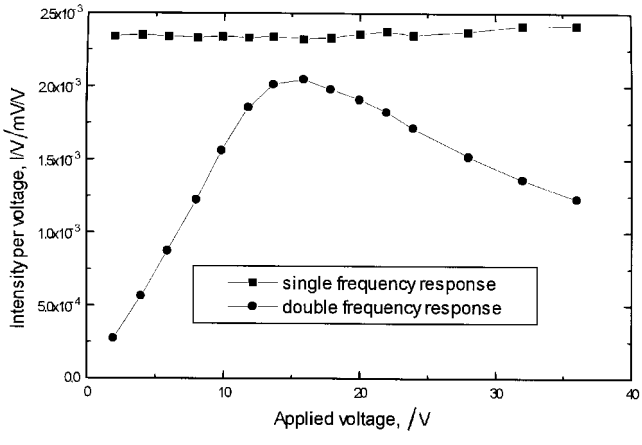

Figure 9. Dependence of the intensity per unit volt (I/V) for the linear and double frequency responses on applied voltage (V) for a well homogeneously aligned 20 μm cell at 75°C; frequency of the applied field 200 Hz.

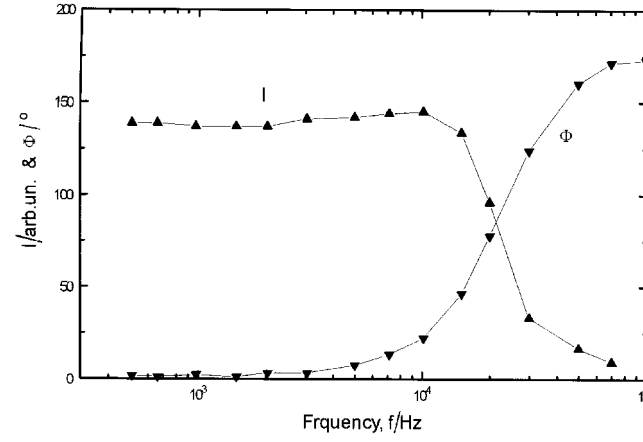

Figure 10. Frequency dependence of intensity (I) and the phase part (Φ) of the linear response for a well homogeneously aligned 20 μm cell at 75°C.

assign this relaxation process in the antiferroelectric phase to the distortion of antiferroelectric order by the electric field caused by a change of angle φ arising from the type of motion shown in figure 4 (*a*). This may also be called 'anti-phase Goldstone mode'. We rule out the assignment due to the soft mode [figure 4 (*b*)] for the reasons given in the previous section.

We may stress that in the literature [8, 9], the mechanism for the lower frequency Process 1 (≈30 kHz) is assigned to the molecular relaxation around the short axis while the higher frequency Process 2 (≈1 MHz) is assigned to the antiferroelectric distortion mode. Our assignment is the reverse. To resolve this contradiction, we examined the results of dielectric and electro-optic spectroscopy given by Hiraoka *et al.* [8]. Elecro-optic spectroscopy up to 100 kHz showed no dependence of the amplitude of the single frequency electro-optic response on frequency as found in our case. This is due to the sufficiently high value of the relaxation frequency of the antiferroelectric distortion mode (1 MHz) which is higher than the high frequency limit of the lock-in amplifier (100 kHz) used in those investigations [8]. Therefore they did not find the single frequency relaxation process in the electro-optic response. On the contrary, the molecular relaxation process around the short axis (Process 1 in [8]) detected in the dielectric spectra below 100 kHz has no electro-optic response. Therefore we conclude that for the samples used in other investigations [8, 9] the relaxation frequency of the molecular relaxation process was lower than that of the antiferroelectric distortion mode, while for our sample the converse is true. This leads us to conclude that the results of electro-optic spectroscopy are extremely important in confirming the mechanism of a collective mode.

For a homogeneously aligned cell, a weak quadratic (double frequency) process is entirely dominated by the

strong linear process and to investigate this non-linear process, completely disoriented cells were prepared. For a cell with random orientations of the directors, the smectic layer normal possesses arbitrary values of the angle between the polarizer axis and the smectic layer normal (angle β), and the linear response is therefore cancelled out through this averaging on the aperture of the light beam. Figure 11 presents the dependence of the amplitude and the phase part of the electro-optic response at double the frequency of the applied signal for an unaligned cell. The relaxation frequency for this process is $\sim$6 kHz, which is twice higher than the frequency of Process 0 in the dielectric spectra. As mentioned before, the relaxation Process 0 is found to exist in the dielectric spectra without bias voltage [6] or only under the bias voltage [5, 8]. We find that for our sample the strength of this process is comparatively low and is screened by the ionic conductivity. Nevertheless by using a fitting program whereby the contributions due to ionic conductivity are subtracted, it is then possible to find the dielectric parameters of this process versus the bias voltage. These results on $\Delta\varepsilon$ are presented in figure 6 and are in agreement with the results published earlier [6]. The non-linear electro-optic response appears to be caused by the distortion of the helix due to the dielectric anisotropy. The relaxation frequency for this response being approximately twice higher than the frequency for Process 0 in the dielectric spectra is in good agreement with theoretical predictions [see equations (16) and (17)]. This process does not exhibit the electro-optic response at the fundamental frequency for the reasons already given. It may be emphasized again that the helical distortion is caused by two mechanisms: polar interactions $\delta\mathbf{PE}$ [figure 4 (*c*)] and the interactions due to the dielectric anisotropy $\Delta\varepsilon\mathbf{E}^2$ [figure 4 (*d*)]. The latter cannot be detected dielectrically, but is clearly observed in the absence of the bias voltage in the electro-optic response at the second harmonic frequency of the applied field. The relaxation frequency for the latter is found to be double those by the polar interactions. The dielectric strength of Process 0 increases initially and follows an increase in the magnitude of $\delta\mathbf{P}$ with the bias voltage. The process is eventually quenched out for higher bias voltages similarly to the bias dependence of the amplitude for the other collective processes.

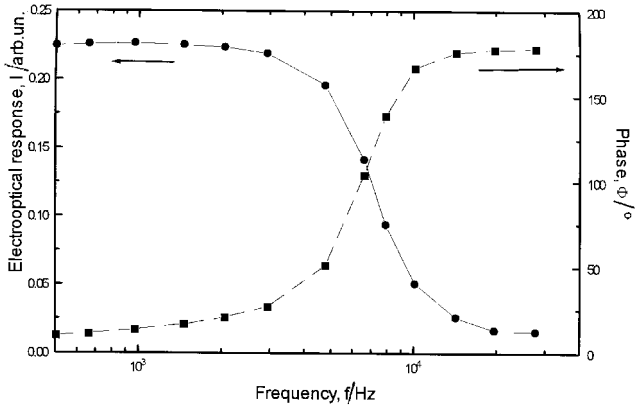

Figure 11. Frequency dependence of the intensity (I) and the phase (Φ) at twice the frequency of the applied signal for an unaligned 20 μm cell at 75°C.

In spite of the fact that both polar and quadratic interactions distort the helix, the relaxation frequency is nevertheless determined by the helical pitch [equations (16) and (17)]. From a complete agreement between the experimental results and the theory given in § 3.3, we unambiguously conclude that the origin of the lowest frequency dielectric relaxation Process 0 and the double frequency electro-optic response lie in the distortion of the antiferroelectric helix and the mode is named the antiferroelectric helix distortion mode.

4. Conclusion

We summarize the findings as follows:

(1) The highest frequency relaxation process (Process 3) is the molecular relaxation around the molecular long axis.

(2) The middle frequency relaxation process (Process 2) is the molecular relaxation around the molecular short axis.

(3) The low frequency relaxation process (Process 1) is due to the distortion of the antiferroelectric order caused by the anti-phase motion shown in figure 4 (*a*). This may appropriately be called the anti-phase antiferroelectric Goldstone mode. It has also been observed in the electro-optic response at the fundamental frequency.

(4) The least frequency relaxation process (Process 0) in the dielectric relaxation spectra is the helical distortion mode. The antiferroelectric Goldstone is suggested to be the appropriate terminology as the mechanism is similar to that of a helical Goldstone mode. The distortion of the helix caused by the dielectric anisotropy gives rise to a non-linear electro-optic response at twice the frequency of the applied field. The reasons for having different frequencies for Process 0, using different measuring techniques, are given by solving an equation that governs the motion of the director of an antiferroelectric helix subject to the weak alternating field.

We thank Prof. J. W. Goodby, Dr A. J. Seed and Dr M. Hird of the University of Hull for useful discussions and for supplying the sample. Forbairt Ireland is acknowledged for partially funding this work.

References

[1] Fukuda, A., Takanishi, Y., Isozaki, T., Ishikawa, K., and Takezoe, H., 1994, *J. mater. Chem.*, **4,** 997.

[2] Isozaki, T., Fujikawa, T., Takezoe, H., Fukuda, A., Hagiwara, T., Suzuki, Y., and Kawamura, I., 1993, *Phys. Rev. B*, **48,** 13 439.

[3] Hiraoka, K., Taguchi, A., Ouchi, Yu., Takezoe, H., and Fukuda, A., 1990, *Jpn. J. appl. Phys.*, **29,** L103.

[4] Moritake, H., Uchiyama, Y., Myojin, K., Ozaki, M., and Yoshino, K., 1993, *Ferroelectrics*, **147,** 53.

[5] Hiller, S., Pikin, S. A., Haase, W., Goodby, J. W., and Nishiyama, I., 1994, *Jpn. J. appl. Phys.*, **33,** L1170.

[6] Buivydas, M., Gouda, F., Lagerwall, S. T., and Stebler, B., 1995, *Liq. Cryst.*, **18,** 879.

[7] Glogarova, M., Stevernyak, H., Nguyen, H. T., and Destrade, C., 1993, *Ferroelectrics*, **147,** 43.

[8] Hiraoka, K., Takezoe, H., and Fukuda, A., 1993, *Ferroelectrics*, **147,** 13.

[9] Merino, S., de la Fuente, M. R., Gonzalez, Y., Perez Jubindo, M. A., and Puertolas, J. A., 1996, *Phys. Rev. E*, **54,** 5169.

[10] Panarin, Yu. P., Kalinovskaya, O., Vij, J. K., and Goodby, J. W., 1997, *Phys. Rev. E*, **55,** 4353.

[11] Orihara, H., Igasaki, Y., and Ishibashi, Y., 1993, *Ferroelectrics*, **147,** 67.

[12] Panarin, Yu. P., Xu, H., MacLughadha, S. T., Vij, J. K., Seed, A. J., Hird, M., and Goodby, J. W., 1995, *J. Phys. condens. Mater.*, **7,** L351; O'Sullivan, J. W., Panarin, Yu. P., Vij, J. K., Seed, A. J., Hird, M., and Goodby, J. W., 1996, *J. Phys. condens. Mater.*, **8,** L551.

[13] Schönfeld, A., and Kremer, F., 1993, *Ber. Bunsenges. phys. Chem.*, **97,** 1237.

[14] De la Fuente, M. R., Jubindo, M. A. P., Zubia, J., Iglesias, T. P., and Seoane, A., 1994, *Liq. Cryst.*, **16,** 1051.

[15] Levstik, A., Kutnjak, Z., Filipič, C., Levstik, I., Bregaz, Z., Zekš, B., and Carlsson, T., 1990, *Phys. Rev. A*, **42,** 2204.

[16] Blinov, L. M., 1983, *Electro-optical and Magneto-optical Properties of Liquid Crystals* (John Wiley), p. 120.

[17] Panarin, Yu. P., Kalinovskaya, O., and Vij, J. K., 1998, *Appl. Phys. Lett.*, **72,** 1667.

[18] Havriliak, S. J., and Negami, S., 1967, *Polym.*, **8,** 101.